Solid Earth Discuss., 1, 93–141, 2009
www.solid-earth-discuss.net/1/93/2009/

Solid Earth Discussions

This discussion paper is/has been under review for the journal Solid Earth (SE).
Please refer to the corresponding final paper in SE if available.

Particle size distributions by laser diffraction – Part 1: Sensitivity of granular matter strength to analytical operating procedures

F. Storti and F. Balsamo

Dipartimento di Scienze Geologiche, Università “Roma Tre”, Largo S. L. Murialdo 1, 00146 Roma, Italy

Received: 6 November 2009 – Accepted: 16 December 2009 – Published: 21 December 2009

Correspondence to: F. Storti (storti@uniroma3.it)

Published by Copernicus Publications on behalf of the European Geosciences Union.

Abstract

We tested laser diffraction particle size analysis in poorly coherent carbonate platform cataclastic breccias and unfaulted quartz-rich eolian sands, representing low- and high-strength granular materials, respectively. We used two different instruments with different sample dispersion and pumping systems and several wet and dry analytical procedures that included different pump speeds, measure precision tests with and without sample ultrasonication, and different dispersant liquids. Results of our work indicate that high strength material is not strongly affected by analytical operating procedures, whereas low strength material is very sensitive to the pump speed, ultrasonication intensity, and measurement run time. To reduce such a data variability, we propose a workflow for analytical tests preliminary to the set up of the most appropriate SOP.

1 Introduction

Particle size distributions provide fundamental information for rock characterization and geological process description in earth sciences, including sedimentology, stratigraphy, structural geology, pedology, and volcanology (e.g. Krumbein, 1941; Irani and Callis, 1963; Engelder, 1974; Friedman, 1979; Sheridan et al., 1987; Rieu and Sposito, 1991). In the last three decades, laser diffraction particle size analysers have proved to be an effective tool for providing particle size distributions of poorly coherent rocks and soils (Weiss and Frock, 1976; McCave et al., 1986; de Boer et al., 1987; Wanogho et al., 1987; Agrawal et al., 1991; Loizeau et al., 1994; Pye and Blott, 2004; Blott and Pye, 2006). This because they need short analysis time and cover a wide size range, and because they require small size samples (e.g. Beuselinck et al., 1998), thus facilitating very detailed studies of particle size distributions in geological structures.

Laser diffraction particle size analysers provide indirect size measurements of spherically equivalent particles, based on the principle that particles of a given size

diffract light through a given angle that increases logarithmically with decreasing size (e.g. Beuselinck et al., 1998). In "wet procedures", few grams of material are dispersed into a liquid that circulates across a quartz measure cell illuminated by a laser beam (Fig. 1). Different instruments have differently designed systems for stirring the dispersant liquid into the tank and ensuring its circulation through the measure cell by mechanical pumping. A wide variety of standard operating procedures (SOP) can be set up in laser diffraction particle size analysers. They include the selection of the pump speed, the number of measurement runs, the length of the measurement time, and the use of dispersant agents and/or ultrasonication to aid sample disaggregation and dispersion (e.g. Blott et al., 2004; Sperazza et al., 2004). It follows that measure results, particularly when dealing with datasets produced by different operators and/or different instruments, can be influenced by the adopted SOP. Sample ultrasonication, for example, can aid particle disaggregation by collision or, in some cases, particle agglomeration (e.g. Mason et al., 2003; Blott et al., 2004).

In this study we analysed particle size distributions of unfaulted quartz-rich (83% quartz, 9% plagioclase, and 8% feldspar) eolian sands from the Priverno quarry, on the Tyrrhenian side of the Central Apennines (e.g. Angelucci and Palmerini, 1961), and carbonate cataclastic breccias from the active Assergi extensional fault system, which bounds to the south the Gran Sasso Massif in the Central Apennines, Italy (e.g. D'Agostino et al., 1998). Our results indicate that particle size data measurement by laser diffraction granulometry is not straightforward in fragile granular materials. We provide an analytical workflow for preliminary testing, propedeutic to final SOP determination in granular rocks.

2 Instruments overview

Most granulometric analyses were performed with a Mastersizer 2000 laser diffraction granulometer and associated dispersion units manufactured by Malvern Instruments Ltd. This laser diffraction particle size analyser is designed for measuring particle

sizes in the 0.02 to 2000 µm range by using a blue (488.0 µm wavelength LED) and red (633.8 µm wavelength He-Ne laser) light dual-wavelength, single-lens detection system. The light energy diffracted by the dilute suspension circulating through the cell is measured by 52 sensors. The light intensity adsorbed by the material is measured as *obscuration* and indicates the amount of sample added to the dispersant liquid. Light scattering data are accumulated in 100 size fractions bins, which are analysed at 1000 readings per second, and compiled with Malvern's Mastersizer 2000 software by using either full Mie or Fraunhofer diffraction theories (de Boer et al., 1987). Light scattering data acquired by the Mastersizer 2000 granulometer were all mathematically inverted with the Mie theory, which utilizes the refractive index (RI) and absorption (ABS) of the dispersed granular material, and RI of the dispersant liquid. This theory is based on the assumption that: (1) particles are homogeneous; (2) particles are spherical; (3) the optical properties of particle and dispersion medium are known; (4) suspension dilution guarantees that light scattered by one particle is measured before being-re-scattered by other particles.

Particle size distributions were measured from wet dispersions using both small (Malvern Hydro 2000 S) and large (Malvern Hydro 2000 MU) volume sample dispersion units available for the Mastersizer 2000 granulometer. The Hydro 2000 S unit has a capacity of 50 to 120 ml and is equipped with a continuously variable single shaft centrifugal pump and stirrer (up to 3500 revolutions per minute; in the following rpm), and by a continuously variable ultrasonic probe. The Hydro 2000 MU unit has a dispersion mechanism consisting of a sample recirculation head immerged into a standard laboratory beaker (capacity of 600 to 1000 ml), which contains a built-in stirrer and sample recirculation centrifugal pump (from 600 to 4000 rpm), and a continuously variable ultrasonic probe (maximum power is 20 µm of tip displacement). A comparative wet analysis was performed by a Cilas 930 laser diffraction granulometer manufactured by Cilas, which measures particle size distributions in the 0.2 to 500 µm size range of wet dispersions by diffraction of a laser light of 830 nm wavelength, based either on the Fraunhofer or Mie diffraction theories. Sample recirculation is achieved by two

peristaltic pumps.

The analysed carbonate fault breccia sample, named CABRE3, was collected in the same site of samples CABRE1 and CABRE2 described in Storti and Balsamo (2009), and was sieved at 500 µm to account for the analytical size range of the Cilas 930 laser diffraction particle size analyser. Reproducible sub-sampling up to about 20 g weight of the total sample amount was achieved by using a Quantachrome sieving riffler-rotary sample splitter. Sub-sample aliquots necessary to produce laser obscuration values between 10% and 15% were randomly selected from sub-samples (from 0.5 g to few grams) and added into the liquid-filled beaker for being analysed.

3 Factors influencing data acquisition and processing from dilute suspensions: testing strategy

Both chemical and mechanical factors can influence light scattering data obtained from dilute suspensions (e.g. Sperazza et al., 2004). Chemical interactions can in fact occur between the dispersion medium, the ~~anlysed~~ material and, possibly, the dispersing agent. Mechanical sample alteration can be produced by two major factors: (i) ultrasonication during sample recirculation and (ii) centrifugal pump and stirrer speed. Moreover, the conversion of light scattering data into particle size distributions depends on the optical properties of both analysed material and dispersant liquid. The high variability of the optical properties of rocks and sediments commonly requires iterative data reprocessing unless essentially monomineralic materials are analysed (e.g. Sperazza et al., 2004).

To investigate on the influence of parameters listed above, we set up the following tests on monomineralic materials like eolian quartz sand (sub-sample aliquots SAND1x) and carbonate cataclastic breccia (sub-sample aliquots CABRE3x): pump speed test, measure precision test (instrument precision test of Blott et al., 2004), ultrasonication test, chemical test, and reprocessing test. The pump speed test is labelled P_t-test, where t is the measurement run time (i.e. the number of readings that

are averaged in a single measurement), and consists of measurement runs performed on a given sub-sample aliquot, at different stirrer and pump speed (in the following simply referred to as pump speed) for a given t. The test starts with the set up of laser obscuration values between 10% and 15% at half of the maximum pump speed. The pump speed is then lowered to the minimum value and few (typically 10) measurement runs are performed before increasing the pump speed (typically by 100 rpm). Progressive measure steps are carried out up to the maximum pump speed. Results are plotted in a mean diameter versus pump speed graph to select the most appropriate rpm value for further analyses. The measure precision test is labelled MPt_S, where S is the pump speed, and consists of measurement runs acquired at given pump speed and measurement run time during sub-sample recirculation through the measure cell. Our MPt_S analyses typically consisted of 100 measurement runs, which means some hundred thousands of instrument readings. Analysis of data trends is included in the measure precision test to help selecting the most appropriate number of measurement runs and to prevent significant mechanical bias. Addition of sub-sample ultrasonication to the measure precision test produces the ultrasonication test US, which is labelled as USd_S, where d is the probe tip displacement in the Hydro 2000 MU dispersion unit. Chemical effects were investigated by repeating the above mentioned sample tests using different dispersion liquids. The suffix / is added to the appropriate test labelling in order to indicate the dispersion liquid used, which can be a solution with a dispersing agent. We did not use specific labelling for decalcified tap water by coupled magnetic and chemical commercial devices, which was used in most of our analyses. The reprocessing test consists of changing the optical properties of both granular material and dispersant liquid during light scattering data processing of a given analysis by the Mie theory through the Mastersizer 2000 software.

The sequential logic of these tests implies that results from one test are then used to properly set up the following ones. Consequently, data interpretation is directly provided in sub-sections associated with the corresponding test descriptions. In most tests, for comparative purposes we acquired 100 measurement runs regardless of indi-

cations from previous tests. This because of the short time required by laser diffraction particle size analysers to acquire light scattering data, thus encouraging the collection of large datasets from which sub-sets can then be easily extracted.

4 Pump speed test

Results of the P_5-test of sub-sample aliquot SAND1a (i.e. 5000 readings of the scattered light energy distribution for each measurement run) are illustrated in Fig. 2. Mean diameters show an asymmetric bell-shaped trend characterized by very low values at 600 and 700 rpm, a maximum at 1000 to 1200 rpm, and an almost flat envelope of mean diameter values at pump speed higher than 1800 rpm (Fig. 2a). The corresponding laser obscuration values show a much higher variability, with a peak at 900 rpm and a minimum at 1300 rpm, followed by a near constant increase at higher pump speed values (Fig. 2b). The trend of D_{10}, D_{50}, and D_{90} percentile data points strongly resembles the distribution of the mean diameters (Fig. 2c). Granulometric curves averaged over 10 measurement runs indicate a strongly unimodal particle size distribution with some variability of both volume percentage and modal peak size between 900 and 1500 rpm. Conversely, almost overlapping curves support strongly consistent results at pump speed values greater than 2000 rpm (Fig. 2d). The well sorted particle size distribution of the sample is illustrated by the pattern of clay, silt, and sand size fractions: starting from 700 rpm, the latter includes 100% of the analysed material (Fig. 2e).

The P_5-test of sub-sample aliquot CABRE3a shows an asymmetric bell-shaped trend characterized by very low values of mean diameters at 600 to 800 rpm, followed by an abrupt increase up to 1100 rpm (Fig. 3a). With increasing the pump speed, mean diameter values rapidly decrease up to 1500 rpm and then continue to overally decrease quite slowly up to the maximum pump speed. The corresponding laser obscuration values show a rapid initial increase up to about 18% at 1000 rpm, followed by a rapid decrease towards the initial reference value (between 14.8% and 15.2%). A short-lived plateau occurs up to 2000 rpm and then obscuration constantly increases with

increasing the pump speed (Fig. 3b). The D_{10}, D_{50}, and D_{90} percentiles show bell-shaped envelopes, qualitatively similar to that of the mean diameter (Fig. 3c). From 2000 to 4000 rpm, the D_{90} data point envelope shows a constant and significant decrease, while D_{50} is characterized by a higher scattering and only a slightly decreasing trend. D_{10} values decrease as well and at 4000 rpm reach almost half of the value at 2000 rpm. Granulometric curves averaged over 10 measurement runs, are characterized by a strongly asymmetric shape that includes a major peak in the coarser fractions and a subordered "long tail" in the finer ones (Fig. 3d). With increasing the pump speed, the height of the major peak decreases and shifts towards finer modal values, and the volume percentage of finer particles (equivalent diameter smaller than about 100 µm) correspondingly increases. The pattern of clay, silt, and sand size fraction curves indicates an initial dominance of silt sizes, followed by their abrupt decrease and a corresponding increase of san size fractions at pump speed values corresponding to the maximum mean diameter values (Fig. 3e). At pump speed values higher than 1500 rpm, the sand size fraction slightly varies about a plateau value, the silt size fraction slightly decreases, and the clay size fraction slightly increases.

Results of the P_1-test of sub-sample aliquot CABRE3b are illustrated in Fig. 4. The overall behaviour of this test is similar to the previous one, with a slightly higher scattering of mean diameter and percentile values. Granulometric curves do not show the almost constant shape evolution that characterizes those acquired at 5 s of measurement run time, despite the overall trend is comparable with the latter.

A comparative P_5-test of sub-sample aliquot CABRE3c was performed with the Hydro 2000 S dispersion unit. The overall behaviour is quite similar to the previous test, with very low mean diameter values at 500 rpm, a maximum at 1200 rpm, and a decrease up to 2000 rpm. The last steps, with pump speed increments of 500 rpm, show quite small variations (Fig. 5a). A P_5-test by the Hydro 2000 S dispersion unit of sub-sample aliquot SAND1b, from 500 to 2500 rpm, shows a bell-shaped distribution of mean diameter values similar to that produced by using the Hydro 2000 MU dispersion unit (Fig. 5b). Comparison of pump speed test results from sample CABRE, acquired at

5s of measurement run time by the Hydro 2000 MU and S dispersion units, shows that the former systematically provides higher mean diameter values at low pump speed ranges up to 1100 rpm, including the highest one (Fig. 5c). In the 1200 to 1600 rpm range, higher mean diameter values are provided by the Hydro 2000 S unit. At higher pump speed, values provided by the two dispersion units are similar.

4.1 Interpretation of the pump speed test results

The meaning of the bell-shaped curve provided by pump speed tests is not straightforward. Low velocity stirring and pumping favour sedimentation of coarser particles at the bottom of the beaker and/or slow motion in the recirculation unit and measure cell, thus producing initial size distributions biased towards the finer particles. The rapid increase of mean diameter values derives from the improved recirculation of progressively coarser particles with increasing the pump and stirrer speed. The highest mean diameter values can either relate to the actual particle size distribution, or to an artefact caused by stagnation/slow motion of coarser material in the measure cell. In the first case, the subsequent decrease of mean diameter values should indicate ongoing particle size reduction, accompanied by a significant increase of laser obscuration at values higher than the initial reference interval. For sub-sample aliquot CABRE3a, such an increase occurs at pump speed values higher than 2100 rpm, whereas obscuration remains almost constant and within the initial reference interval from 1500 to 2000 rpm (Fig. 3b). This evidence suggests that highest mean diameter values are coarseward biased by ineffective sample recirculation, and that values in the plateau characterizing both mean diameter and laser obscuration values, correspond to the most likely measurement runs. In CABRE3b the obscuration data point plateau adjacent to the maximum value is not well developed and, conversely, it seems indicating a slight increase of finer material during measurement. However, analysis of the D_{10}, D_{50}, and D_{90} percentiles does not indicate significant particle size reduction despite significant scattering.

The behaviour of obscuration values associated with sub-sample aliquot SAND1a is

different and this can relate to the different rock type and size. Initial values very close to zero can be explained by the very good sorting of the sample, almost totally consisting of sand-size particles that, at very low pump speed, are almost entirely deposited at the bottom of the beaker. The constant increase of laser obscuration values at pump speed higher than 1300 rpm indicates an increase of the material amount in the dispersion unit. Percentiles, however, would support much smaller size variations (Fig. 2c). This apparently contrasting evidence can be reconciled by admitting an increase of very fine particles and negligible overall particle size reduction. The source of such extremely fine grained material is likely collision-induced surface polishing of quartz grains, which are originally coated by iron hydroxide thin films imparting them a slightly orange colour. The same colour characterized water in the beaker at the end of the analyses.

Results from the pump speed tests illustrated above can be schematically explained by a composite trend of mean values as a function of pump speed values, where four major stages can be identified (Fig. 6): (1) an initial segment characterized by very low mean diameter values, which is interpreted to indicate fineward bias by ineffective material recirculation into the dispersion unit and measure cell; (2) the adjacent, bell-shaped segment containing the maximum mean diameter values, which is interpreted to indicate coarseward bias by ineffective material recirculation; (3) the third, flat-lying or slowly dipping segment, which is interpreted to indicate effective material recirculation without significant mechanical alteration, thus providing the most effective pump speed size range for further analyses; (4) the fourth segment, characterised by progressively decreasing mean diameter values indicating the occurrence of significant mechanical alteration and consequent fineward biasing of the sample material data.

5 Measure precision test

Results from the pump speed test on the SAND1 sample indicate negligible influence of this parameter for values higher than 2000 rpm. We performed a $MP2500_5$ test (i.e. 2500 rpm of pump speed and 5s of measurement run time) on sub-sample aliquot

SAND1c (Fig. 7). Mean diameter values ~~maintain extremely similar during~~ the 100 runs, ~~as well as~~ D_{10}, D_{50}, and D_{90} percentiles, while obscuration values are scattered and progressively increase. Granulometric curves selected to monitor the evolution of the test show virtually identical shapes, as supported by the very low variations of the corresponding mode values (Fig. 7d). This indicates that no material finer than sand was produced during measurement runs (Fig. 7e).

The pump speed test for sample CABRE3 indicates that 2000 rpm is the most suitable pump speed value to ensure effective material recirculation without very invasive mechanical alteration. Moreover, 5 s of measurement run time are expected to provide more statistically robust results than 1 s. Accordingly, we initially performed a $MP2000_5$, test on sub-sample aliquot CABRE3d (Fig. 8). Mean diameter values show significant scattering and a slightly decreasing trend with time, while laser obscuration progressively increased. The value of D_{50}, and D_{90} percentiles show a pattern similar to the mean diameter, being the scattering of the former particularly higher. On the other hand, D_{10} percentile values are extremely small. Selected granulometric curves are quite similar apart from the first run one (Fig. 8d). The corresponding modal values show a much higher mode for the first run, followed by a drop of about 140 µm in the second one. Slightly higher values characterize runs 3 to 5, and then very similar values pertain to the following runs (about 350 µm) with the exception of the last one, which has a higher mode, slightly higher than 400 µm. The distribution of sand, silt and clay size fractions show a scattered pattern about a slightly decreasing trend for the sand size, less scattering about a slightly increasing trend for the silt size, and negligible scattering about near constant values for the clay size fraction (Fig. 8e).

Data from MP tests at 1200 rpm and 4000 rpm pump speed, respectively, performed for comparative purposes on the influence of pump speed, are illustrated in Fig. 9. The first test is characterized by extremely high data scattering, whereas in the second case scattering is quite small, average diameter values are lower, and laser obscuration values increase at higher rate than the corresponding ones acquired at 2000 rpm. Comparative measure precision tests designed to investigate on the influence of mea-

surement run time were performed at 2000 rpm of pump speed and 1 s, 10 s, 20 s, and 40 s of measurement run time, respectively. The $MP2000_1$, test on sub-sample aliquot CABRE3g (Fig. 10) is characterized by intense scattering of mean diameter values that show an increasing trend with increasing the run number (i.e. time). Intense scattering also occurs in D_{50}, and D_{90} percentiles and in the sand, silt and clay size fraction data. The selected granulometric curves show a higher variability and a non systematic trend, compared to the corresponding ones acquired at 5 s of measurement run time, as also indicated by the corresponding modal values (Fig. 10d). For a constant total duration of the measure precision test, increasing the measurement run time causes a decrease of mean diameter data scattering and more linearly increasing trends of laser obscuration values (Fig. 11). We also run a MP_5 test on sub-sample aliquot CABRE3k by using the Cilas 930 laser diffraction particle size analyser. Results provided significantly smaller mean diameter values with respect to those provided by the Mastersizer 2000, and these values systematically decreased through time, as indicated by the very good linear best fit (Fig. 12).

Plotting mean diameters of test $MP2000_5$ averaged every five measurement runs, indicates a progressive decrease of values with time. In particular, such a decrease can be effectively fitted by an exponential curve, and the highest variation occurs between the first two points (Fig. 13a). A similar trend characterizes the corresponding modal values, despite higher scattering (Fig. 13b). A detail of laser obscuration data for the first ten runs shows a very slight, almost linear increase, which reaches about 1% at the end of the test (Fig. 13c). The corresponding granulometric curves indicate that only the first and third runs provided coarser distributions, with a modal peak of about 510 µm, while the remaining eight ones are quite similar and have a modal peak of about 400 µm that remains unchanged also after 50 and 100 runs (Fig. 13d). In particular, the third run curve provides the coarsest distribution, and the corresponding D_{10}, D_{50}, and D_{90} percentiles and modal value are outliers with respect to the overall trend of the other data (Fig. 13e–g). This evidence questions the validity of the third run data.

5.1 Interpretation of the measure precision test results

The measure precision test provided contrasting results depending on the rock type. Carbonate cataclastic breccias are sensitive to the material recirculation time (i.e. the number of measurement runs and/or the measurement run time), whereas eolian sand data remains almost unaltered through time. In particular, in carbonate cataclastic breccias a significant difference occurs between the first run and the following ones, suggesting that only short recirculation times ensure a small mechanical bias to particle size data from wet suspension analyses.

6 Ultrasonication test

An ultrasonication test on eolian sand was performed on sub-sample aliquot SAND1d, using the maximum ultrasonication probe tip displacement (20 µm), 2500 rpm of pump speed, and 5 s of measurement run time ($US20_5$). Mean diameters remain almost constant in the first 26 runs, with an average value of 270.8 µm, and then suddenly steps down to an average value of 262.3 µm in the remaining 73 runs of the test. The average value over 100 runs is 264.5 µm (Fig. 14a). Laser obscuration values increase of about 12.5% during the test (Fig. 14b). When only the first 10 granulometric curves are compared, they show a virtually constant modal peak at about 259 µm. The corresponding volume percentage drops ~~of~~ about 1.75% from curve 7 onward (Fig. 14c). Modal values remain almost constant for the entire test, about an average value of 258.5 µm (Fig. 14d). Contrasting these 10 curves from the ultrasonication test, against the first one from the measure precision test on sub-sample aliquot SAND1c indicates negligible differences(Fig. 14c).

Ultrasonication intensities of 2.5 µm, 5 µm, 10 µm, and 20 µm of tip displacement were applied to the carbonate cataclastic breccia, using a pump speed of 2000 rpm and 5 s of measurement run time. Results indicate that increasing the ultrasound energy causes (i) a faster decrease of mean diameter values, which passes from linear

to power law best fit curves, (ii) higher increases of laser obscuration, and (iii) a decrease of average modal values up to 10 µm, which remain almost constant when the maximum probe tip displacement is used (Fig. 15). Analysis of granulometric curves pertaining to the first 10 runs and to runs 50 and 100 in each test shows a progressively increasing difference between first run curves and the remaining ones with increasing the ultrasonication probe tip displacement (Fig. 16). Moreover, shape differences among curves increase, particularly between test $US2.5_5$ and the remaining ones, and the modal peak volume percentage of the bulk of the curves in each test decreases with increasing ultrasonication intensity. Comparison of the first run curves from test with and without ultrasonication shows that the latter provide a significantly coarser particle size distribution in the modal peak (Fig. 16e). The influence of ultrasonication is also illustrated by the difference between first-run modal values and those averaged over the first 10 runs of the corresponding tests. The greater difference occurs when no ultrasonication was used. The smaller difference occurs at the minimum ultrasonication intensity and then it increases up to the $US10_5$ test.

6.1 Interpretation of the ultrasonication test results

Results from ultrasonication tests indicate negligible effects on eolian sand, particularly when only the first 10 to 20 runs are considered, according to the measure precision test evidence. On the other hand, in the carbonate cataclastic breccia sub-sample aliquots, ultrasonication has a much greater influence causing significant particle size reductions after few measurement runs, as indicated by the concomitant reduction of mean diameter and mode values, by the increase of laser obscuration, and by the increase of volume percentages in the 0.5 µm to 100 µm segments of granulometric curves. Even after a single measurement run, ultrasonication is able to reduce the modal peak value of particle size distributions ~~of about 60 µm to 80 µm~~.

7 Chemical test

The influence of denaturated ethylic alcohol on data acquisition from eolian sand was investigated by performing a MP2500$_{5al}$, test on sub-sample aliquot SAND1e. Results are very consistent, as illustrated by the almost constant mean diameter values, by the flat lying best fit line of mode values, and by the very similar granulometric curves in the first 10 runs, which provide an extremely good overlap with the first curve from the same test using decalcified tap water as dispersant liquid (Fig. 17). The corresponding modal values show an initial decrease of less than 5 µm, reaching a plateau value after 4 runs.

Two measure precision tests were performed on CABRE3p and CABRE3q sub-sample aliquots, using denaturated ethylic alcohol and demineralised water, respectively (Fig. 18). The first test provided quite scattered mean diameter and mode values, both characterized by flat-lying best fit lines, which are smaller than the corresponding ones obtained from demineralised water of about 70 µm and 53 µm, respectively. The increase of laser obscuration values is greater for the dispersion in denaturated ethylic alcohol. Analysis of granulometric curves pertaining to the first 10 runs indicates a higher variability for measurements acquired in denaturated ethylic alcohol, of both curve shape and modal peak elevation (Fig. 18g, h). Such a higher variability is confirmed by the analysis of the corresponding modal values. Finally, comparison with the first run curve from the same test using decalcified tap water as dispersant liquid, indicates that granulometric curves obtained from the denaturated ethylic alcohol suspension have much greater differences with respect to the corresponding ones acquired using demineralised water as dispersant liquid.

7.1 Interpretation of the chemical test results

Test results indicate that the use of denaturated ethylic alcohol has a negligible influence on data acquisition in quartz eolian sand. Variations of mean diameter and mode values are less than 5 µm, which fall inside the variability associated with sub-

sampling, even in well sorted sediments like dune sands. On the other hand, the same dispersant liquid causes a decrease of about 75 µm of mean diameter values when carbonate cataclastic breccia is analysed. The evidence that, when demineralised water is used, results are very similar to those from the corresponding test in decalcified tap water rules out any significant bias produced by sub-sampling and supports particle fragmentation during suspension recirculation. This is well illustrated by the systematic decrease of modal peak volumes and size, and by the corresponding increase of volume percentage values in the 0.5 µm to 110 µm segments of granulometric curves in Fig. 18g. Higher variations occur after only two runs.

8 Reprocessing test

Following from previous ~~test~~ 1, on sub-sample aliquot SAND1c was selected for data reprocessing. Changing RI values from 1.4 to 1.8 causes negligible effects in eolian quartz sand, as illustrated in Fig. 19. The corresponding granulometric curves almost perfectly overlap and percentiles and modal values show a very small variability. The same result was obtained when varying ABS values from 1.00 to 0.01 (Fig. 20). Changing RI in carbonate cataclastic breccia (first run of test $MP2000_5$ on sub-sample aliquot CABRE3d) causes some variability in the corresponding grain size distributions, particularly from RI=1.4 to RI=1.6 (Fig. 21). Analysis of residuals associated with best fit curves indicates that the most appropriate RI value is 1.6. Higher values, however, do not significantly influence the computed particle size distributions, as lower values do particularly for the volume percentage of sizes lower than about 2 µm (Fig. 21b). The major effect of changing ABS values from 1.00 to 0.01 on CABRE material is to progressively shorten the tail of granulometric curves, from about 0.25 µm (ABS=1.00–0.50) to 0.6 µm when ABS=0.01 (Fig. 22). For ABS lower than 1.00, decreasing particle absorption causes an increase of percentile values and a decrease of modal values. Analysis of residuals associated with best fit curves indicates that the most appropriate ABS value is 0.01. Finally, changing the RI value of the dispersant liquid has negligible

effects on eolian quartz sand, and an influence on CABRE material that is comparable to what produced by changing RI of carbonate particles (Fig. 23).

8.1 Interpretation of reprocessing test results

Results of these tests indicate that in the case of the analyzed materials, the sensitivity of light scattering data reprocessing by the Mie theory is mainly governed by the particle size range, rather than by their optical properties. In fact, the very good sorting of sample SAND1 results in a virtually insensitive behavior to reprocessing, while the large spanning of sizes in CABRE3 enhances the sensitivity of particles finer that about 2 µm.

9 Discussion

Results illustrated above indicate that particles with different strength respond in a very different way to the same testing strategy during particle size determination by laser diffraction. Quartz eolian sand provided virtually identical particle size distributions regardless of the adopted operating procedure. On the other hand, carbonate cataclastic breccia is very sensitive to operating procedures. Such a contrast indicates that the variability associated with the sample CABRE3 does not depend on instrumental bias, but instead it relates to the peculiar fabric of cataclastic rocks derived from massive protoliths like platform carbonates. In fact, in this case particles are produced by multiple fracturing, rolling and grinding of material within fault zones (e.g. Borg et al., 1960; Storti et al., 2003; Sammis and Ben Zion, 2008). Particle size depends on the relative strength distribution along cleavage and microfracture sets as a function of the applied stress (e.g. Sammis et al., 1987). Accordingly, the mechanical behaviour of these carbonate cataclastic particles can be compared to that of sedimentary particles made of cohesive aggregate grains. Conversely, multiple collisions of quartz particles during eolian transport along coastal dunes ensures effective exploiting of pre-existing

flaws. The resulting rounded particles are strong enough for being not significantly influenced by mechanical solicitations in laser diffraction particle size analysers.

It follows that determining the appropriate operating procedure bears a fundamental importance for heavily microfractured materials, while it has secondary effect when high strength particles are analysed. In the latter case, only pump speed can influence the final results by not ensuring effective particle recirculation in the dispersion unit. However, given the high strength of this material, pump speed values close or higher than half of maximum speed (e.g. 2000–3000 rpm) can be used without expecting any significant mechanical bias. On the other hand, operating procedures as less invasive as possible are required when analysing fragile granular materials. In this case, finding the proper analytical workflow benefits of some general guidelines for broad sample categories, followed by further specific refinements. Moreover, selecting an effective instrumentation plays a fundamental role to determine particle size distributions of fragile materials. According to our tests, peristalting pumping during sample recirculation introduces a systematic bias to the final results and, consequently, laser diffraction analysers adopting this technical solution are inappropriate. On the other hand, centrifugal pumping provides a much more flexible and effective solution for analysing fragile materials. Between the two Malvern dispersion units we used, the large volume Hydro 2000 MU ensured effective sample recirculation at lower pump speed values compared to the Hydro 2000 S.

Our preferred workflow (Fig. 24) starts with a pump speed test to provide indications on the pump speed range for further testing. Short measurement run times (typically 5 s as a starting value) are used in pump speed analyses, in order to minimise subsample mechanical alteration without compromising the statistical robustness of the data. Results from the P-test provide constraints for MP and US test pairs performed at the same pump speed values. More than one test pair can be performed to investigate uncertainties associated with the pump test. Cross checking of results from the MP and US tests is commonly achieved by comparing the behaviour of mean diameters, of the corresponding laser obscuration values, and of other statistical parameters including

the mode and percentiles, among which D_{10}, D_{50}, and D_{90} are the most common ones. Once the most appropriate parameters in terms of best sample recirculation, measure run time, and measure run number are selected, all information for defining the most appropriate SOP is available for a given dispersion liquid. The next step is to check the effectiveness of the selected dispersion medium by running the same test with different dispersion liquids. Comparison of all results leads to the selection of the final SOP, which can be repeated for several sub-samples to perform a sampling precision test (Blott et al., 2004) that allows evaluating measure reproducibility (Fig. 24). It is worth nothing that, despite the effectiveness of statistical parameters like mean diameter, percentiles, and others, they cannot replace the use of granulometric curves for comparing results from different tests. This because very similar average values can relate to very different granulometric curves (e.g. Selley, 2000).

10 Conclusions

Particle size distributions significantly contribute to the description of many geological processes including sedimentation, rock fragmentation and soil formation. Modern laser diffraction particle size analysers ensure fast data acquisition over a wide size range, coupled with the appropriate flexibility for analysing very different granular materials. This flexibility, however, can produce severely biased results when inappropriate analytical operating procedures are used, particularly on fragile materials. We analysed both high strength (eolian quartz sand) and low strength (carbonate cataclastic breccia) essentially monomineralic materials to test the impact of different analytical operating procedures involving particle dispersion into a liquid, on the obtained particle size distributions. Our results can be summarised by the following points:

1. centrifugal pumping the particle-liquid dilute dispersion at the most appropriate pump speed is crucial in wet analyses of granular material to prevent (i) dramatic underestimating coarser particles when ineffective pumping and stirring allow particle sedimentation; (ii) overestimating coarser particles when ineffective pumping

and stirring allow transient particle stagnation within the measure cell; (iii) underestimating coarser particles when fast pumping and stirring produce significant particle size reduction in low strength material during measure running;

2. high strength material is not significantly influenced by the adopted instrumentation and standard operating procedure, provided that effective sample recirculation is obtained in the dispersion unit;

3. adding ultrasonication in wet analyses of low strength material systematically causes mechanical particle size reduction during ~~measure running~~ that, however, is less effective than ~~what~~ caused by fast pumping and stirring during sample recirculation and mainly produces very fine particles by polishing of the larger ones;

4. in low strength material, the number of averaged measurement runs has to be carefully determined by statistical data analysis of large datasets in order to ensure robust outputs and minimize mechanical biasing of particle size during recirculation in the dispersion unit;

5. Selecting appropriate optical properties for the analysed sample material and dispersant liquid, respectively, is particularly important for fine and very fine particles, ~~being~~ coarser ~~ones~~ less affected by this parameter.

We propose a workflow as a guideline for addressing particle size determinations by laser diffraction granulometry. Application of this procedure is typically flexible due to the great variability of analysed materials and the common need of several iterations before reaching the most statistically robust results. Systematic support of laser diffraction granulometric data by preliminary test results performed to select the adopted operating procedure is necessary. The lack of information on this can contribute to misleading data interpretation and data comparison.

Acknowledgements. We are grateful to R. M. Joeckel for his helpful review of the submitted manuscript. Constructive criticism and advice from S. Blott on an early version of the manuscript were very useful for significantly improving it. Funding for this work was provided by the "Roma Tre" University Laboratory Upgrade Programme, grants to F. Storti, and by the Italian MIUR (Ministero dell'Istruzione, dell'Università e della Ricerca). L. Aldega, C. Giampaolo and S. Lo Mastro kindly provided the composition of the Priverno sand by X-ray diffraction. We are grateful to Malvern Instruments Ltd. (particularly to B. Floure, P. Kippax and A. Virden) and to Alfatest s.r.l. (particularly to M. Congia and V. Polchi) for their technical support and advice. This paper is dedicated to the memory of Renato Funiciello, who inspired and encouraged our work during these years.

References

Agrawal, Y. C., McCave, I. N., and Riley, J. B.: Laser diffraction size analysis, in: Principles, Methods and Application of Particle Size Analysis, edited by: Syvitski, J. P. M., Cambridge University Press, Cambridge, 119–128, 1991.

Angelucci, A. and Palmerini, V.: Studio sedimentologico delle sabbie rosse di Priverno (Lazio sud-occidentale), Geologica Romana, 3, 203–225, 1961.

Beuselinck, L., Govers, G., Poesen, J., Degraer, G., and Froyen, L.: Grain-size analysis by laser diffractometry: comparison with the sieve-pipette method, Catena, 32, 193–208, 1998.

Blott, S. J., Croft, D. J., Pye, K., Saye, S. E., and Wilson, H. E.: Particle size analysis by laser diffraction, in: Forensic Geoscience: Principles, Techniques and Applications, edited by: Pye, K. and Croft, D. J., Geological Society, London, Special Pubblication, 232, 63–73, 2004.

Blott, S. J. and Pye, K.: Particle size distribution analysis of sand-size particles by laser diffraction: an experimental investigation of instrument sensitivity and the effects of particle shape, Sedimentology, 53, 671–685, 2006.

Borg, I., Friedman, M., Handin, J., and Higgs, D. V.: Experimental deformation of S. Peter sand: a study of cataclastic flow, Geol. Soc. Am. Mem., 79, 133–191, 1960.

D'Agostino, N., Chamot-Rooke, N., Funiciello, R., Jolivet, L., and Speranza, F.: The role of pre-existing thrust faults and topography on the styles of extension in the Gran Sasso range (central Italy), Tectonophysics, 292, 229–254, 1998.

de Boer, G. B. J., de Weerd, C., Thoenes, D., and Goossens, H. W. J.: Laser diffraction spectrometry: Fraunhofer diffraction versus Mie scattering, Particle Characterization, 4, 138–146, 1987.
Engelder, J. T.: Cataclasis and the generation of fault gouge, Geol. Soc. Am. Bull., 85, 1515–1522, 1974.
Friedman, G. M.: Differences in size distributions of populations of particles among sands of various origins, Sedimentology, 26, 3–32, 1979.
Irani, R. R. and Callis, C. F.: Particle size: measurements, interpretation, and application, John Wiley and Sons, New York, 1963.
Krumbein, W. C.: Measurement and geologic significance of shape and roundness of sedimentary particles, J. Sed. Petr., 11, 64–72, 1941.
Loizeau, J. L., Arbouille, D., Santiago, S., and Vernet, J. P.: Evaluation of a wide range laser diffraction grain size analyzer for use with sediments, Sedimentology, 41, 353–361, 1994.
Mason, J. A., Jacobs, P. M., Greene, R. S. B. and Nettleton, W. D.: Sedimentary aggregates in the Peoria Loess of Nebraska, USA, Catena, 53, 377–397, 2003.
McCave, I. N., Bryant, R. J., Cook, H. F. and Coughanowr, C. A.: Evaluation of a laser-diffraction-size analyzer for use with natural sediments, J. Sed. Petr., 56, 561–564, 1986.
Pye, K. and Blott, S. J.: Particle size analysis of sediments, soils and related particulate materials for forensic purposes using laser granulometry, Forensic Science Int., 144, 19–27, 2004.
Rieu, M. and Sposito, G.: Fractal fragmentation, soil porosity and soil water properties: I. Theory, Soil Sci. Soc. Am. J., 55, 1231–1238, 1991.
Sammis, C. G. and Ben Zion, Y.: Mechanics of grain-size reduction in fault zones, J. Geophys. Res., 113, B02306, doi:10.1029/2006JB004892, 2008.
Sammis, C. G., King, G., and Biegel, R.: The kinematics of gouge deformation, Pure Appl. Geophys., 125, 777–812, 1987.
Selley, R. C.: Applied Sedimentology, second edition, Academic Press, SanDiego, 2000.
Sheridan, M. F., Wohletz, K. H., and Dehn, J.: Discrimination of grain-size sub-populations in pyroclastic deposits, Geology, 15, 367–370, 1987.
Sperazza, M., Moore, J. N., and Hendrix, M. S.: High-resolution particle size analysis of naturally occurring very fine-grained sediment through laser diffractometry, J. Sedim. Res., 74, 736–743, 2004.
Storti, F., Billi, A., and Salvini, F.: Particle size distributions in natural carbonate fault rocks:

insights for non-self-similar cataclasis, Earth Planet. Sci. Lett., 206, 173–186, 2003.
Wanogho, S., Gettinby, G., and Caddy, B.: Particle size distribution analysis of soils using laser diffraction, Forensic Science Int., 33, 117–128, 1987.
Weiss, E. L. and Frock, H. N.: Rapid analysis of particle-size distributions by laser light scattering, Powder Technology, 14, 287–293, 1976.

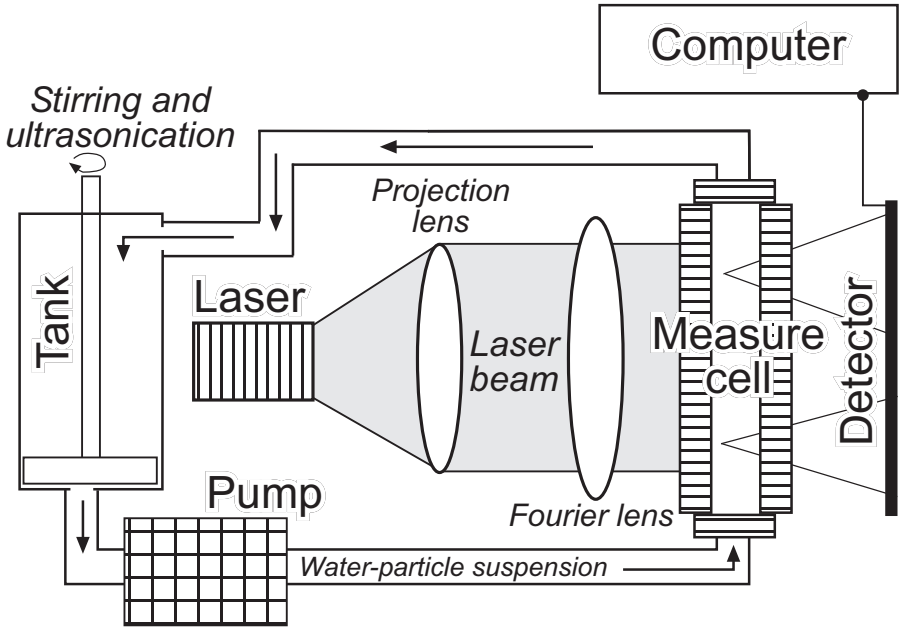

Fig. 1. Schematic cartoon showing the main components of a laser diffraction particle size analyzer. See text for details.

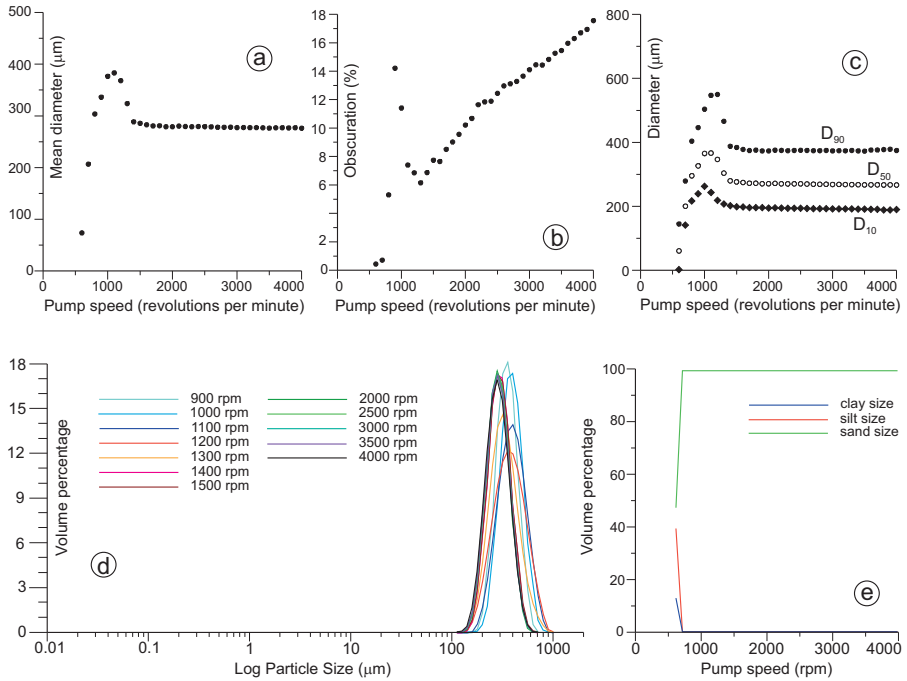

Fig. 2. Results of the pump speed test P_5 performed on sub-sample aliquot SAND1a by the Hydro 2000 MU dispersion unit. **(a)** Mean diameter value evolution with increasing the pump speed from 600 up to 4000 rpm. **(b)** Laser obscuration value progression during the same test. **(c)** Progression of D_{10}, D_{50}, and D_{90} percentiles during the same test. **(d)** Granulometric curves obtained by averaging data from the corresponding 10 measurement runs during representative pump speed steps. **(e)** Distribution of clay, silt, and sand size fractions during the test. Note that the sand fraction quickly reaches 100% of the sample material. See text for details.

SED
1, 93–141, 2009

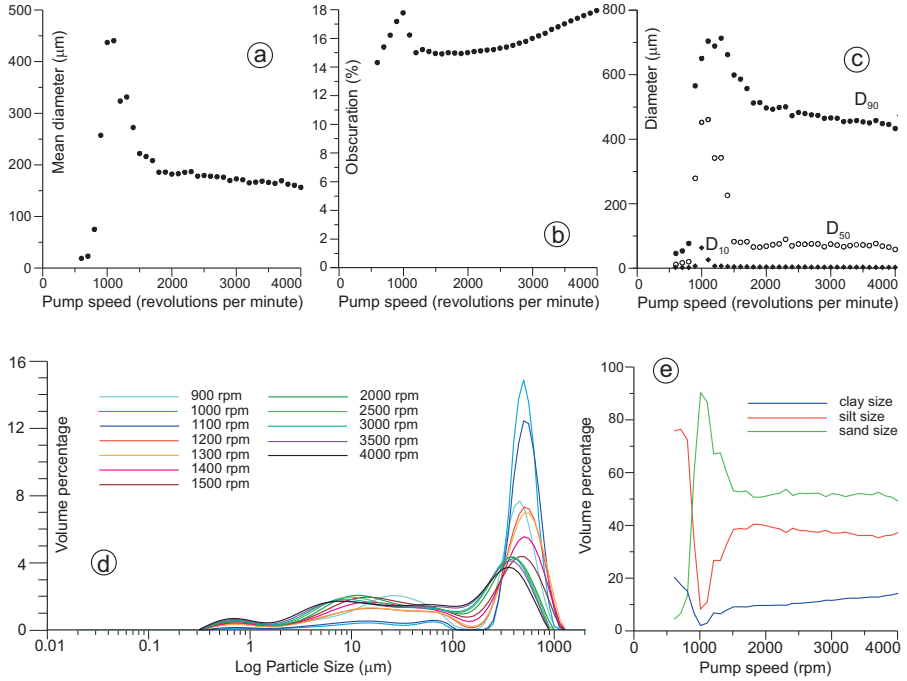

Fig. 3. Results of the pump speed test P_5 performed on sub-sample aliquot CABRE3a by the Hydro 2000 MU dispersion unit. **(a)** Mean diameter value evolution with increasing the pump speed from 600 up to 4000 rpm. **(b)** Laser obscuration value progression during the same test. **(c)** Progression of D_{10}, D_{50}, and D_{90} percentiles during the same test. **(d)** Granulometric curves obtained by averaging data from the corresponding 10 measurement runs during representative pump speed steps. **(e)** Distribution of clay, silt, and sand size fractions during the test.

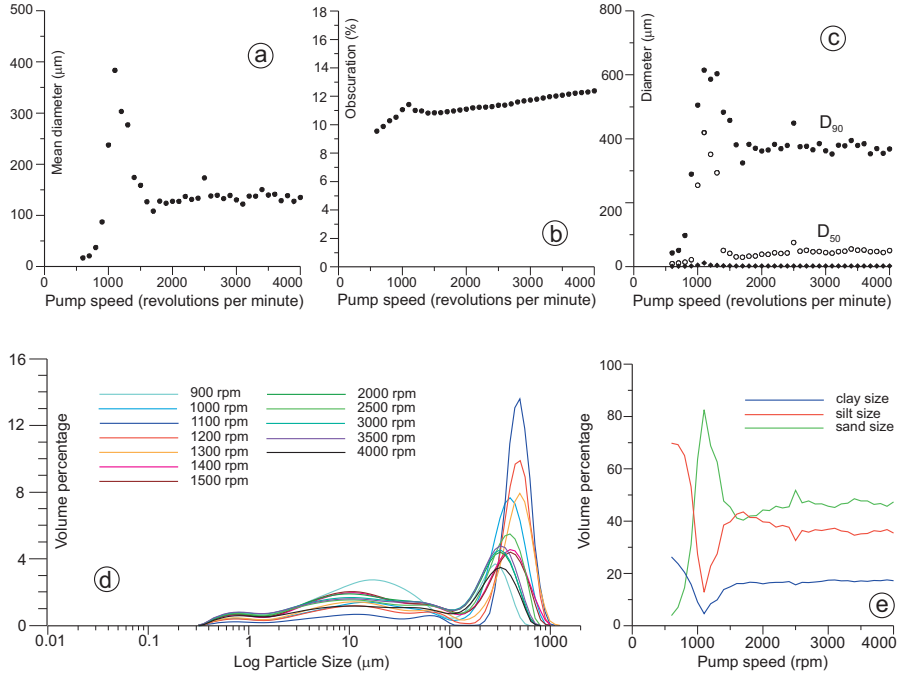

Fig. 4. Results of the pump speed test P_1 performed on sub-sample aliquot CABRE3b by the Hydro 2000 MU dispersion unit. **(a)** Mean diameter value evolution with increasing the pump speed from 600 up to 4000 rpm. **(b)** Laser obscuration value progression during the same test. **(c)** Progression of D_{10}, D_{50}, and D_{90} percentiles during the same test. **(d)** Granulometric curves obtained by averaging data from the corresponding 10 measurement runs during representative pump speed steps. **(e)** Distribution of clay, silt, and sand size fractions during the test.

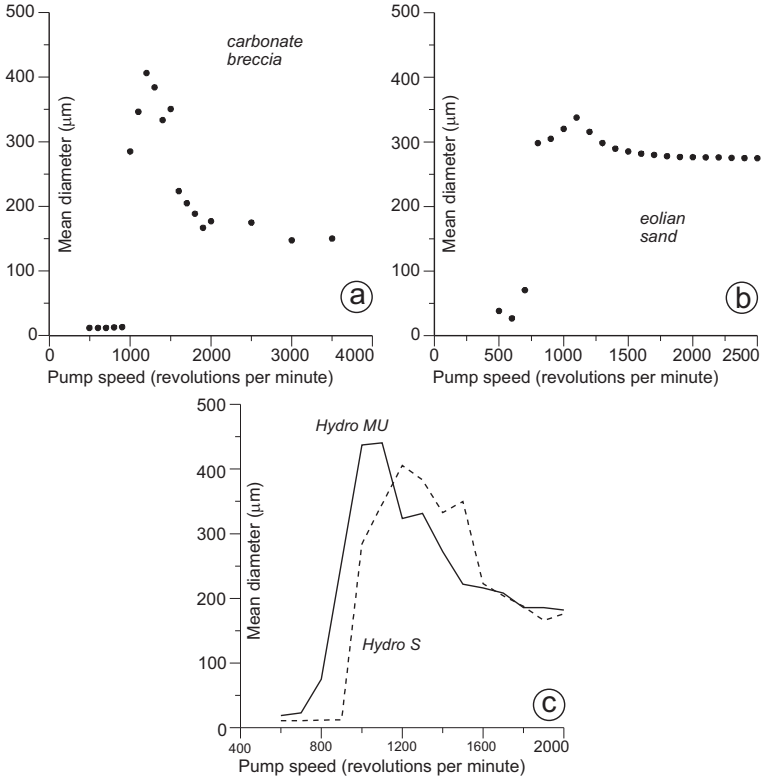

Fig. 5. **(a)** Pump speed test P_5 performed on sub-sample aliquot CABRE3c by the Hydro 2000 S dispersion unit; mean diameter value evolution with increasing the pump speed from 500 up to 3500 rpm. **(b)** Pump speed test P_5 performed on sub-sample aliquot SAND1b by the Hydro 2000 S dispersion unit; mean diameter value evolution with increasing the pump speed from 500 up to 2500 rpm. **(c)** Comparison, in ~~the~~ 500–2000 rpm, of the trends of mean diameter values obtained from pump speed tests on sample CABRE. The solid line refers to data in Fig. 3a; the broken line refers to data in Fig. 5a.

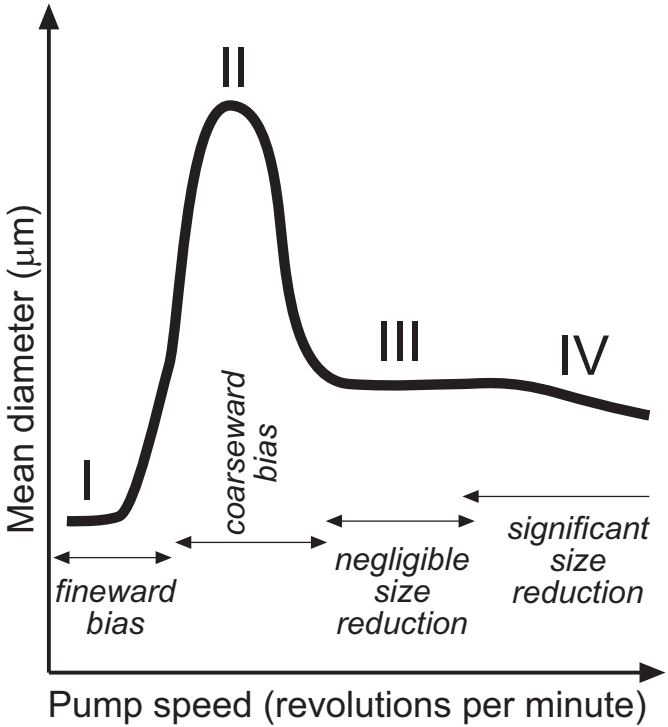

Fig. 6. Conceptual sketch showing the four main stages characterizing the typical asymmetric bell shaped curve resulting from the progression of mean diameter values during pump speed tests of granular materials. See text for details.

SED
1, 93–141, 2009

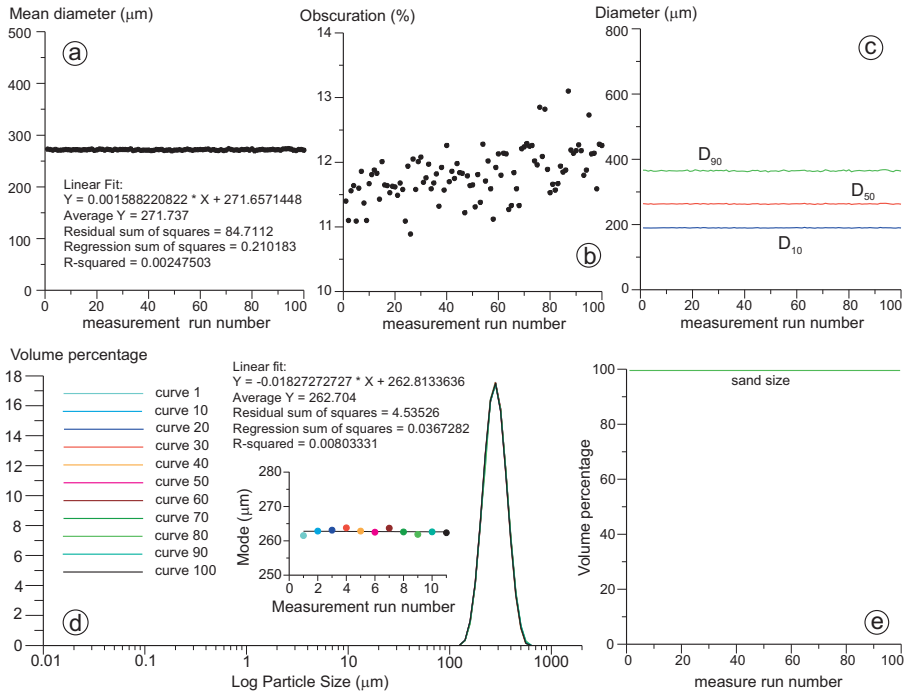

Fig. 7. Results of the measure precision test $MP2500_5$ performed on sub-sample aliquot SAND1c by the Hydro 2000 MU dispersion unit. **(a)** Mean diameter value evolution with increasing the number of measurement runs. Data statistics is provided. **(b)** Laser obscuration value progression during the same test. **(c)** Progression of D_{10}, D_{50}, and D_{90} percentiles during the same test. **(d)** Granulometric curves representative of the particle size evolution. Note their virtually perfect overlap. The corresponding modal values (same colour code) are illustrated in the inset graph, whose statistics is also provided. Note how average modal and mean values are very similar. **(e)** Distribution of the sand size fractions during the test. It represents 100% of the sample, without any significant amount of clay and silt.

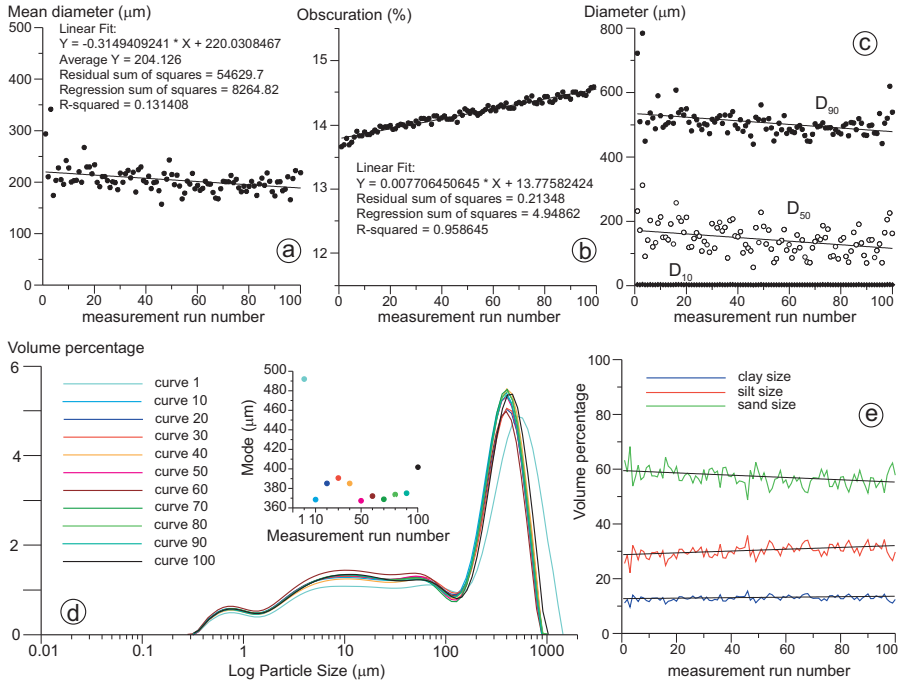

Fig. 8. Results of the measure precision test $MP2000_5$ performed on sub-sample aliquot CABRE3d by the Hydro 2000 MU dispersion unit. **(a)** Mean diameter value evolution with increasing the number of measurement runs. Data statistics is provided. **(b)** Laser obscuration value progression during the same test. Data statistics is provided. **(c)** Progression of D_{10}, D_{50}, and D_{90} percentiles during the same test. **(d)** Granulometric curves representative of the particle size evolution. The corresponding modal values (same colour code) are illustrated in the inset graph. **(e)** Distribution of the clay, silt and sand size fractions during the test.

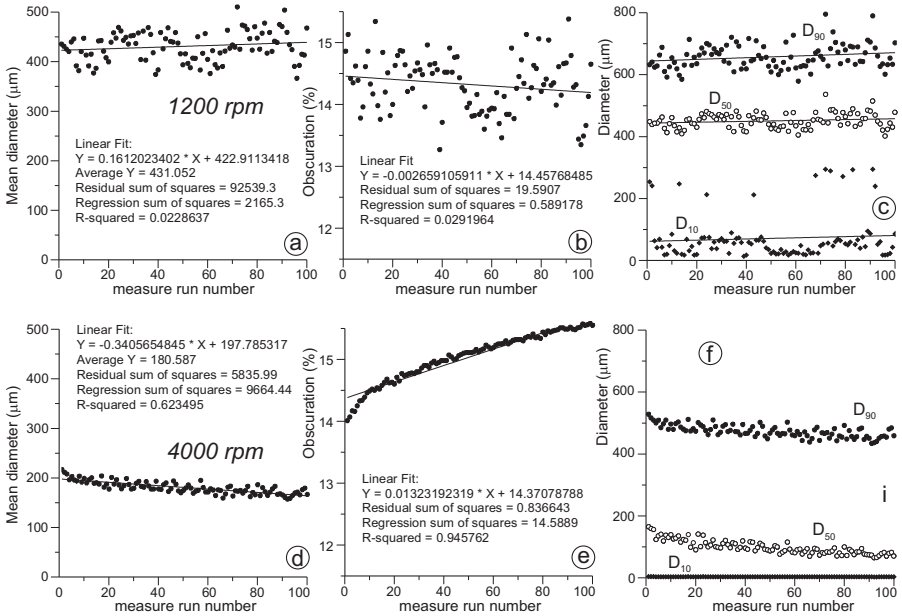

Fig. 9. Comparison between measure precision test results performed on sample CABRE3 at the pump speed corresponding to the mean diameter peak value of the pump speed test (Fig. 3a), and at the maximum pump speed, respectively. **(a)** Test $MP1200_5$ performed on sub-sample aliquot CABRE3e by the Hydro 2000 MU dispersion unit; mean diameter value evolution with increasing the number of measurement runs. Data statistics is provided. **(b)** Laser obscuration value progression during the same test. Data statistics is provided. **(c)** Progression of D_{10}, D_{50}, and D_{90} percentiles during the same test. **(d)** Test $MP4000_5$ performed on sub-sample aliquot CABRE3f by the Hydro 2000 MU dispersion unit; mean diameter value evolution with increasing the number of measurement runs. Data statistics is provided. **(e)** Laser obscuration value progression during the same test. Data statistics is provided. **(f)** Progression of D_{10}, D_{50}, and D_{90} percentiles during the same test. Note the very large difference between the average mean diameter obtained from the first (431.052 µm) and the second test (180.587 µm), respectively. Both them are affected by strong recirculation-related mechanical bias.

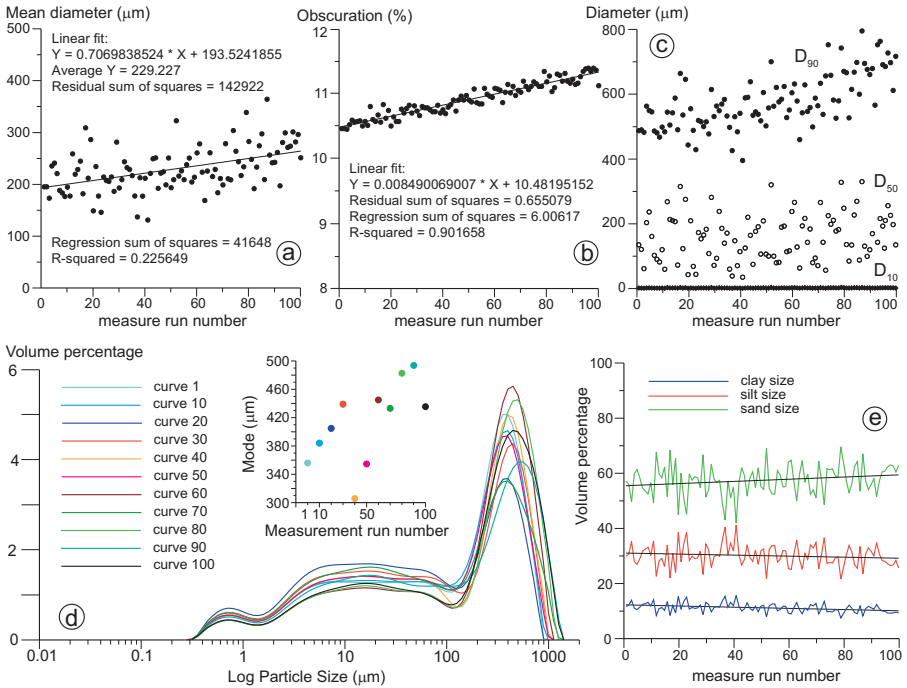

Fig. 10. Results of the measure precision test MP2000$_1$ performed on sub-sample aliquot CABRE3g by the Hydro 2000 MU dispersion unit. **(a)** Mean diameter value evolution with increasing the number of measurement runs. Data statistics is provided. **(b)** Laser obscuration value progression during the same test. Data statistics is provided. **(c)** Progression of D_{10}, D_{50}, and D_{90} percentiles during the same test. **(d)** Granulometric curves representative of the particle size evolution. The corresponding modal values (same colour code) are illustrated in the inset graph. **(e)** Distribution of the clay, silt and sand size fractions during the test.

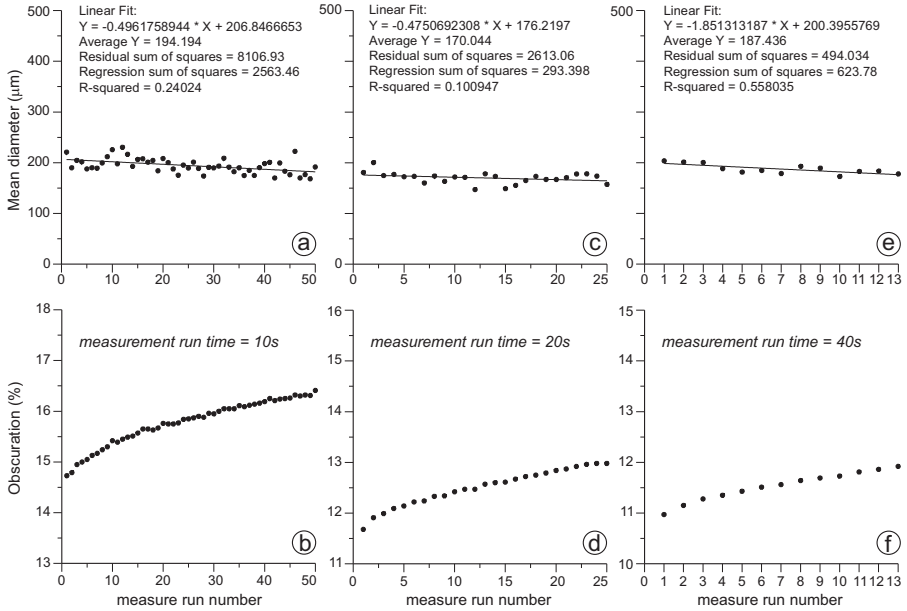

Fig. 11. Results of measure precision tests performed at different run times on sample CABRE3 by the Hydro 2000 MU dispersion unit. **(a)** Test $MP2000_{10}$ on sub-sample aliquot CABRE3h; mean diameter value evolution with increasing the number of measurement runs. Data statistics is provided. **(b)** Laser obscuration value progression during the same test. Data statistics is provided. **(c)** Test $MP2000_{20}$ on sub-sample aliquot CABRE3i; mean diameter value evolution with increasing the number of measurement runs. Data statistics is provided. **(d)** Laser obscuration value progression during the same test. Data statistics is provided. **(e)** Test $MP2000_{40}$ on sub-sample aliquot CABRE3j; mean diameter value evolution with increasing the number of measurement runs. Data statistics is provided. **(f)** Laser obscuration value progression during the same test. Data statistics is provided.

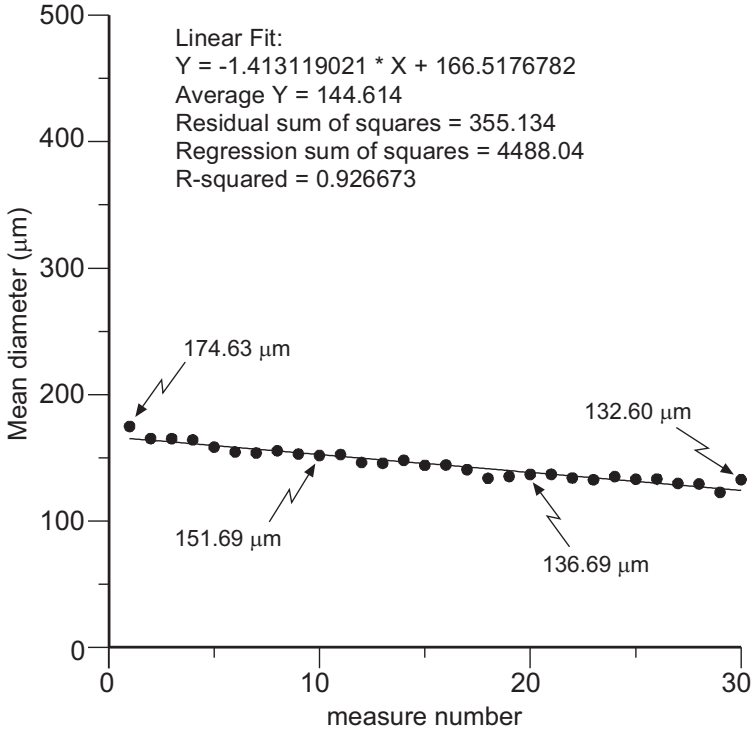

Fig. 12. Results of a measure precision tests performed on sub-sample aliquot CABRE3k by the Cilas 930 laser diffraction particle size analyser; mean diameter value evolution with increasing the number of measurement runs. Data statistics is provided.

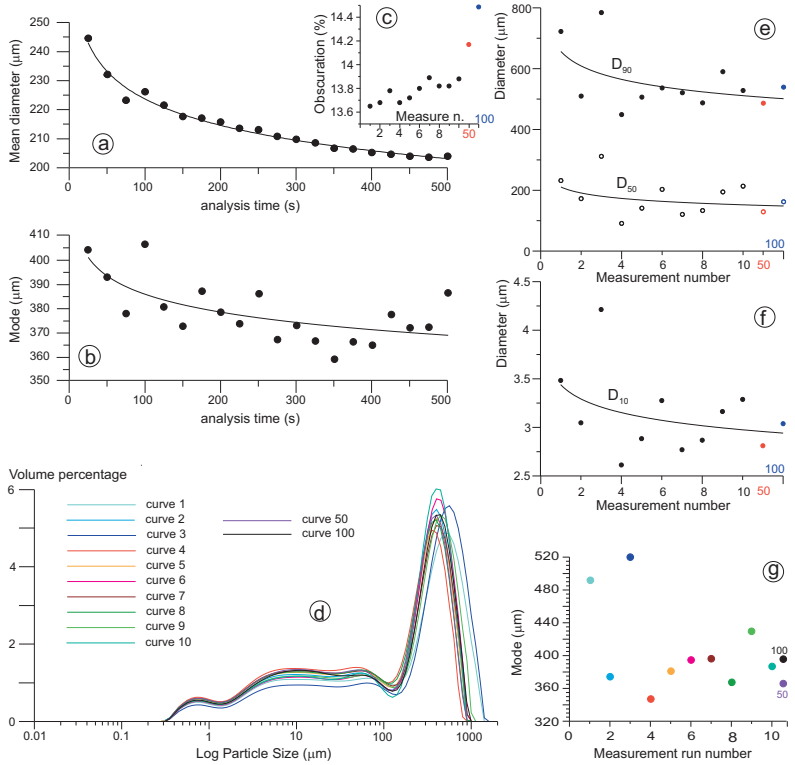

Fig. 13. Analysis of data from the test $MP2000_5$ on sub-sample aliquot CABRE3d (Fig. 8). **(a)** Mean diameter values averaged every five measurement runs. **(b)** Average modal values corresponding to data in (a). In both cases, the best fits indicate an exponential decay. **(c)** Laser obscuration values recorded during the first 10 runs (black dots), compared with the values after 50 (red dot) and 100 (blue dot) measurement runs. **(d)** Granulometric curves computed for the first 10 runs, compared with the ones from the 50th and 100th run. **(e)** Progression of D_{50} and D_{90} percentiles during the first 10 measurement runs. Data after 50 (red dot) and 100 (blue dot) runs are provided for comparison. **(f)** Progression of D_{10} percentiles during the first 10 measurement runs. Data after 50 (red dot) and 100 (blue dot) runs are provided for comparison. **(g)** Progression of modal values during the first 10 measurement runs (colour code as in d). Data after 50 (grey dot) and 100 (black dot) runs are provided for comparison.

SED
1, 93–141, 2009

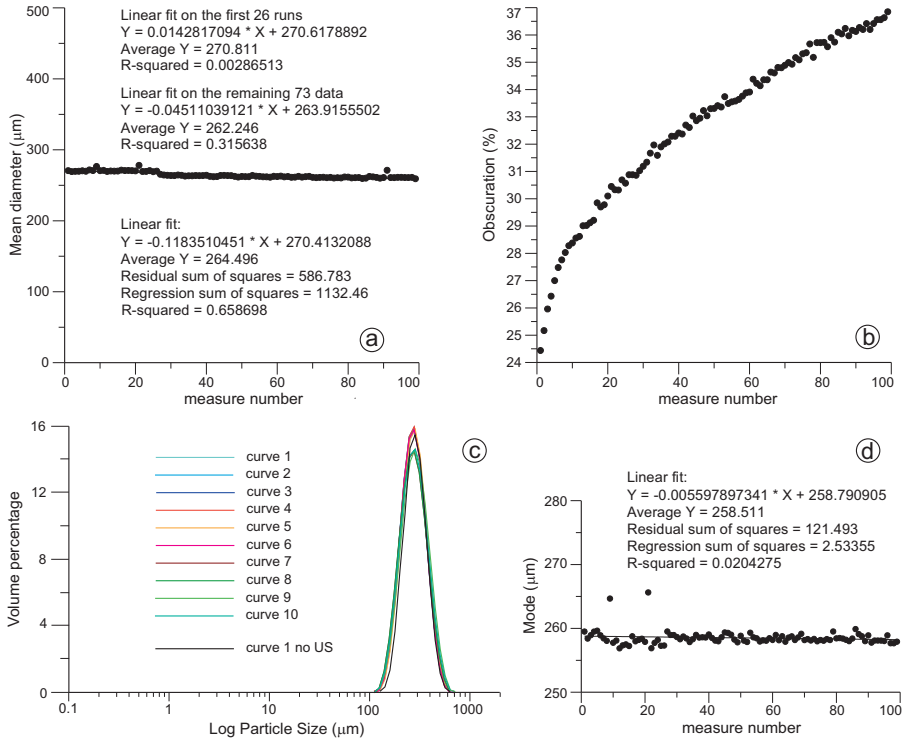

Fig. 14. Results of the ultrasonication test $US20_5$ performed on sub-sample aliquot SAND1d by the Hydro 2000 MU dispersion unit. **(a)** Mean diameter value evolution with increasing the number of measurement runs. Data statistics is provided for the cumulative dataset, for the first 26 runs, and for the remaining 73 runs, respectively. **(b)** Laser obscuration value progression during the same test. **(c)** Granulometric curves computed for the first 10 runs, compared with the first curve from the test $MP2500_5$ on sub-sample aliquot SAND1c (Fig. 7). Progression of modal values with increasing the number of measurement runs. Data statistics is provided.

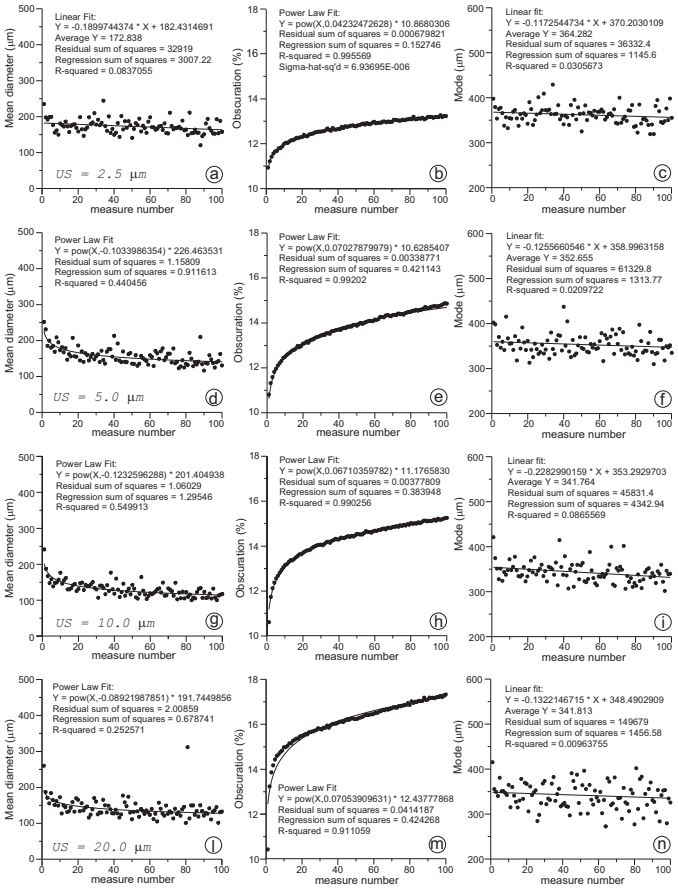
Linear Fit:
Y = -0.1899744374 * X + 182.4314691
Average Y = 172.838
Residual sum of squares = 32919
Regression sum of squares = 3007.22
R-squared = 0.0837055
Mean diameter (µm)
US = 2.5 µm
measure number
Power Law Fit:
Y = pow(X,0.04232472628) * 10.8680306
Residual sum of squares = 0.000679821
Regression sum of squares = 0.152746
R-squared = 0.995569
Sigma-hat-sq'd = 6.93695E-006
Obscuration (%)
measure number
Linear fit:
Y = -0.1172544734 * X + 370.2030109
Average Y = 364.282
Residual sum of squares = 36332.4
Regression sum of squares = 1145.6
R-squared = 0.0305673
Mode (µm)
measure number
Power Law Fit
Y = pow(X,-0.1033986354) * 226.463531
Residual sum of squares = 1.15809
Regression sum of squares = 0.911613
R-squared = 0.440456
Mean diameter (µm)
US = 5.0 µm
measure number
Power Law Fit:
Y = pow(X,0.07027879979) * 10.6285407
Residual sum of squares = 0.00338771
Regression sum of squares = 0.421143
R-squared = 0.99202
Obscuration (%)
measure number
Linear fit:
Y = -0.1255660546 * X + 358.9963158
Average Y = 352.655
Residual sum of squares = 61329.8
Regression sum of squares = 1313.77
R-squared = 0.0209722
Mode (µm)
measure number
Power Law Fit:
Y = pow(X,-0.1232596288) * 201.404938
Residual sum of squares = 1.06029
Regression sum of squares = 1.29546
R-squared = 0.549913
Mean diameter (µm)
US = 10.0 µm
measure number
Power Law Fit:
Y = pow(X,0.06710359782) * 11.1765830
Residual sum of squares = 0.00377809
Regression sum of squares = 0.383948
R-squared = 0.990256
Obscuration (%)
measure number
Linear fit:
Y = -0.2282990159 * X + 353.2929703
Average Y = 341.764
Residual sum of squares = 45831.4
Regression sum of squares = 4342.94
R-squared = 0.0865569
Mode (µm)
measure number
Power Law Fit:
Y = pow(X,-0.08921987851) * 191.7449856
Residual sum of squares = 2.00859
Regression sum of squares = 0.678741
R-squared = 0.252571
Mean diameter (µm)
US = 20.0 µm
measure number
Power Law Fit
Y = pow(X,0.07053909631) * 12.43777868
Residual sum of squares = 0.0414187
Regression sum of squares = 0.424268
R-squared = 0.911059
Obscuration (%)
measure number
Linear fit:
Y = -0.1322146715 * X + 348.4902909
Average Y = 341.813
Residual sum of squares = 149679
Regression sum of squares = 1456.58
R-squared = 0.00963755
Mode (µm)
measure number

Fig. 15.

Fig. 15. Ultrasonication tests on sample CABRE3 by the Hydro 2000 MU dispersion unit. **(a)** ultrasonication test $US2.5_5$ performed on sub-sample aliquot CABRE3l; mean diameter value evolution with increasing the number of measurement runs. **(b)** Laser obscuration value progression during the same test. **(c)** Mode value progression during the same test. **(d)** ultrasonication test $US5_5$ performed on sub-sample aliquot CABRE3m; mean diameter value evolution with increasing the number of measurement runs. **(e)** Laser obscuration value progression during the same test. **(f)** Mode value progression during the same test. **(g)** ultrasonication test $US10_5$ performed on sub-sample aliquot CABRE3n; mean diameter value evolution with increasing the number of measurement runs. **(h)** Laser obscuration value progression during the same test. **(i)** Mode value progression during the same test. **(l)** ultrasonication test $US20_5$ performed on sub-sample aliquot CABRE3o; mean diameter value evolution with increasing the number of measurement runs. **(m)** Laser obscuration value progression during the same test. **(n)** Mode value progression during the same test. Data statistics is provided for all plots.

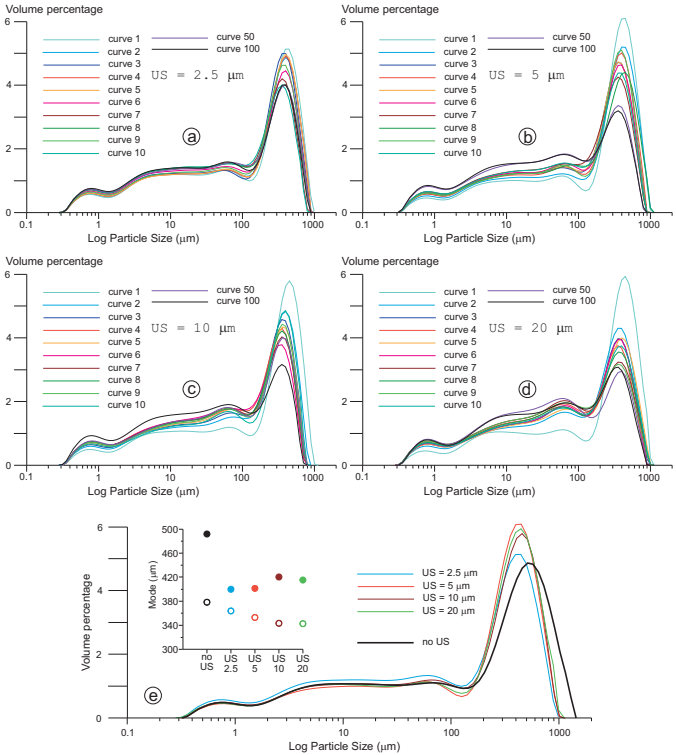

Fig. 16. **(a)** Granulometric curves computed for the first 10 runs of test US2.5$_5$ performed on sub-sample aliquot CABRE3l, compared with the ones from the 50th and 100th run. **(b)** Granulometric curves computed for the first 10 runs of test US5$_5$ performed on sub-sample aliquot CABRE3m, compared with the ones from the 50th and 100th run. **(c)** Granulometric curves computed for the first 10 runs of test US10$_5$ performed on sub-sample aliquot CABRE3n, compared with the ones from the 50th and 100th run. **(d)** Granulometric curves computed for the first 10 runs of test US20$_5$ performed on sub-sample aliquot CABRE3o, compared with the ones from the 50th and 100th run. **(e)** First run granulometric curves from the four tests listed above, compared with the first run curve from test MP2000$_5$ on sub-sample aliquot CABRE3d (Fig. 8). The inset graph shows the modal values of the same first run cuves (filled dots, same colour code) compared with modal values averaged over the first 10 runs of the corresponding tests (empty dots, same colour code).

SED
1, 93–141, 2009

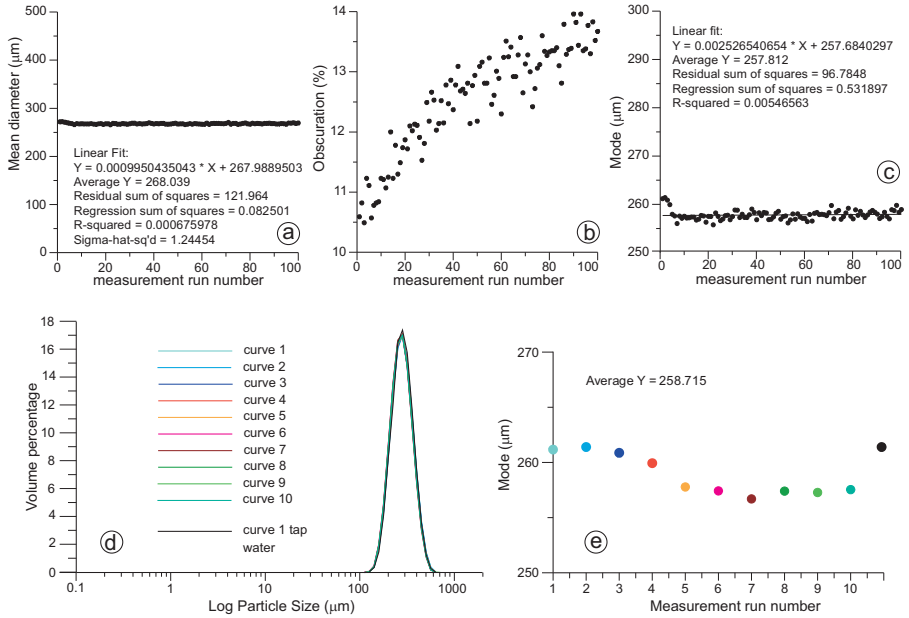

Fig. 17. Results of the chemical test MP2500$_{5al}$ performed on sub-sample aliquot SAND1e by the Hydro 2000 MU dispersion unit, using denaturated ethylic alcohol as dispersant liquid. **(a)** Mean diameter value evolution with increasing the number of measurement runs. Data statistics is provided. **(b)** Laser obscuration value progression during the same test. **(c)** Progression of modal values with increasing the number of measurement runs. Data statistics is provided. **(d)** Granulometric curves computed for the first 10 runs, compared with the first curve from the test MP2500$_5$ on sub-sample aliquot SAND1c (Fig. 7). **(e)** Modal values corresponding to the curves in (d).

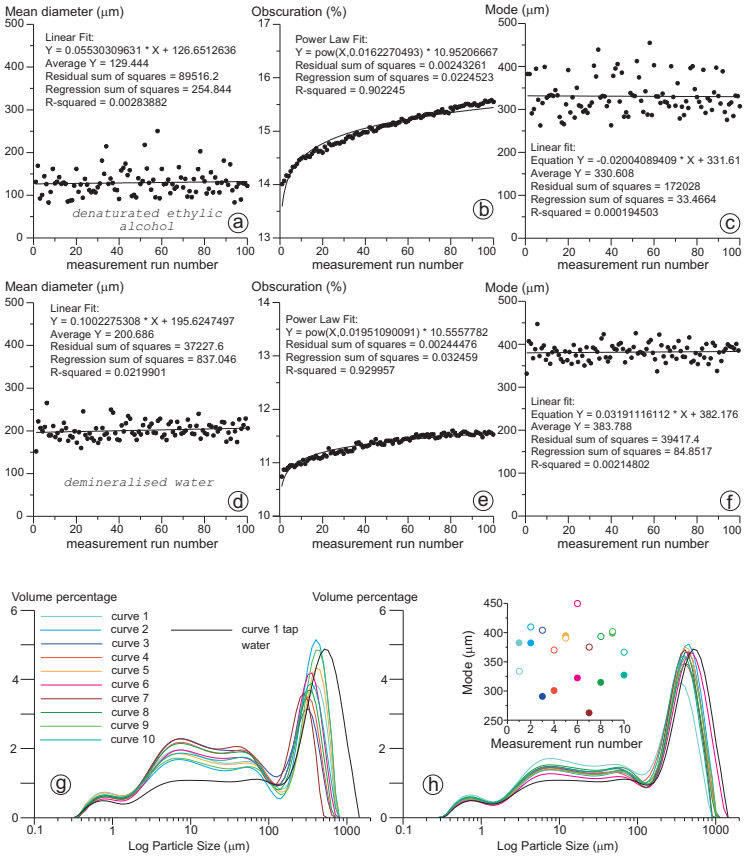
Mean diameter (μm)
Linear Fit:
Y = 0.05530309631 * X + 126.6512636
Average Y = 129.444
Residual sum of squares = 89516.2
Regression sum of squares = 254.844
R-squared = 0.00283882
denaturated ethylic alcohol
a
Obscuration (%)
Power Law Fit:
Y = pow(X,0.0162270493) * 10.95206667
Residual sum of squares = 0.00243261
Regression sum of squares = 0.0224523
R-squared = 0.902245
b
Mode (μm)
Linear fit:
Equation Y = -0.02004089409 * X + 331.61
Average Y = 330.608
Residual sum of squares = 172028
Regression sum of squares = 33.4664
R-squared = 0.000194503
c
measurement run number
Mean diameter (μm)
Linear Fit:
Y = 0.1002275308 * X + 195.6247497
Average Y = 200.686
Residual sum of squares = 37227.6
Regression sum of squares = 837.046
R-squared = 0.0219901
demineralised water
d
Obscuration (%)
Power Law Fit:
Y = pow(X,0.01951090091) * 10.5557782
Residual sum of squares = 0.00244476
Regression sum of squares = 0.032459
R-squared = 0.929957
e
Mode (μm)
Linear fit:
Equation Y = 0.031911116112 * X + 382.176
Average Y = 383.788
Residual sum of squares = 39417.4
Regression sum of squares = 84.8517
R-squared = 0.00214802
f
measurement run number
Volume percentage
curve 1
curve 2
curve 3
curve 4
curve 5
curve 6
curve 7
curve 8
curve 9
curve 10
curve 1 tap water
g
Log Particle Size (μm)
Volume percentage
Mode (μm)
Measurement run number
h
Log Particle Size (μm)

Fig. 18.

Fig. 18. Results of chemical tests performed on sample CABRE3e by the Hydro 2000 MU dispersion unit. **(a)** Test $MP2000_{5al}$ performed on sub-sample aliquot CABRE3p using denaturated ethylic alcohol as dispersant liquid; mean diameter value evolution with increasing the number of measurement runs. Data statistics is provided. **(b)** Laser obscuration value progression during the same test. Data statistics is provided. **(c)** Progression of modal values with increasing the number of measurement runs. Data statistics is provided. **(d)** Test $MP2000_{5dw}$ performed on sub-sample aliquot CABRE3q using demineralised water as dispersant liquid; mean diameter value evolution with increasing the number of measurement runs. Data statistics is provided. **(e)** Laser obscuration value progression during the same test. Data statistics is provided. **(f)** Progression of modal values with increasing the number of measurement runs. Data statistics is provided. **(g)** Granulometric curves computed for the first 10 runs in (a), compared with the first curve from the test $MP2000_5$ on sub-sample aliquot CABRE3d (Fig. 8). **(h)** Granulometric curves computed for the first 10 runs in (d), compared with the first curve from the test $MP2000_5$ on sub-sample aliquot CABRE3d (Fig. 8). The inset graph shows the comparison between modal values corresponding to the curves in (g) (filled dots) and in (h) (empty dots).

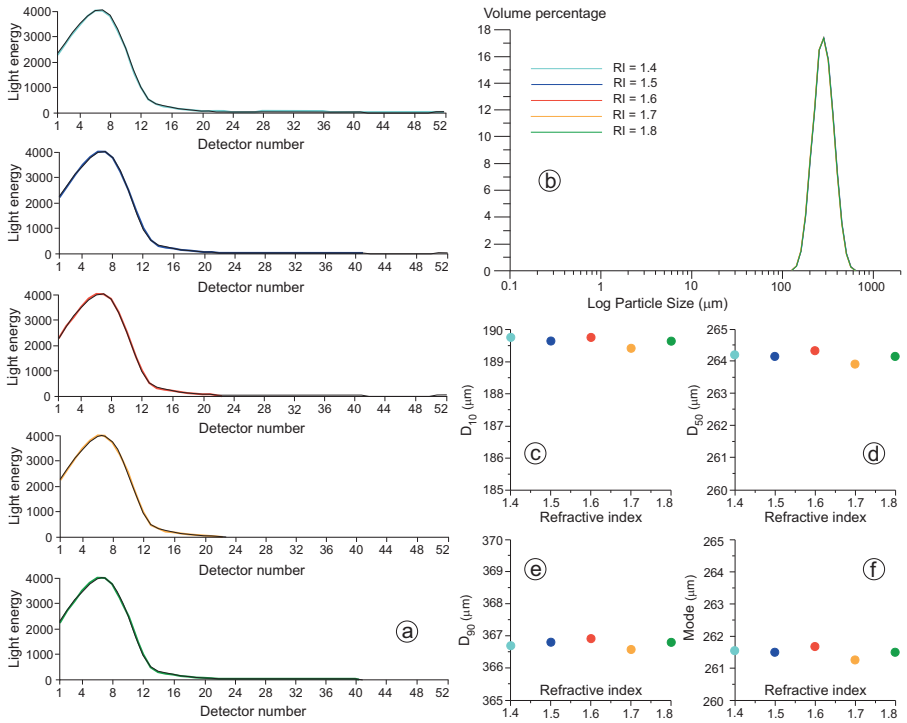

Fig. 19. Reprocessing of the first run data from test MP2500$_5$ on sub-sample aliquot SAND1c (Fig. 7). **(a)** Light scattering data (black curve) and corresponding best fits for variable RI values of quartz from 1.4 to 1.8 (colour code in b), constant ABS values of quartz=0.1, and constant RI values of decalcified tap water=1.33. **(b)** Granulometric curves computed from reprocessed data in (a). **(c)** D_{10} percentiles for data in the 5 curves illustrated in (b). **(d)** D_{50} percentiles for data in the 5 curves illustrated in (b). **(e)** D_{90} percentiles for data in the 5 curves illustrated in (b). **(f)** Modal values for data in the 5 curves illustrated in (b). It is worth noting that changing RI of quartz produces negligible changes in the reprocessed data.

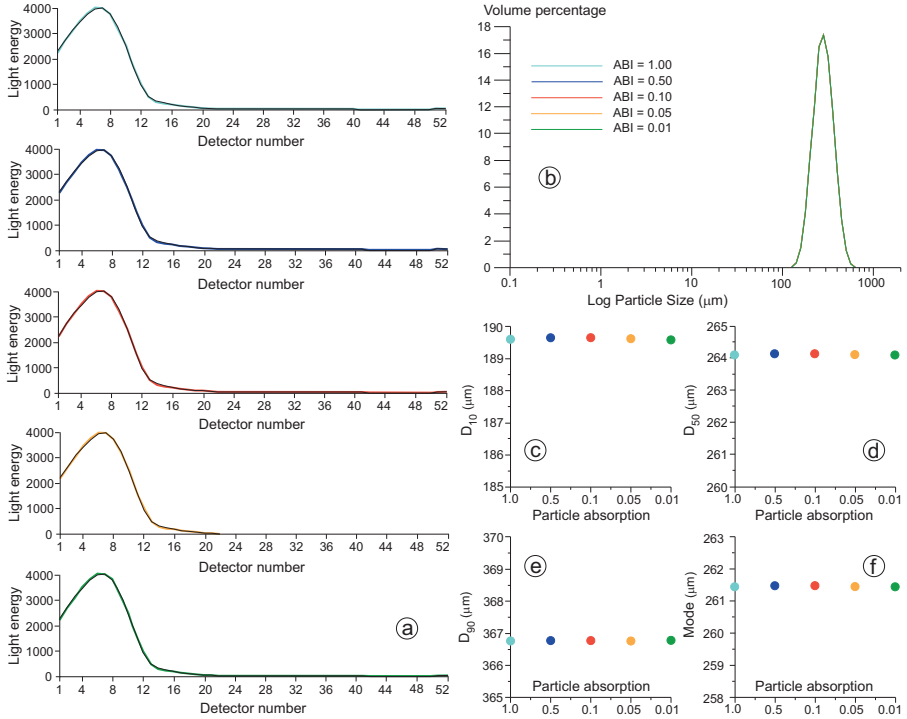

Fig. 20. Reprocessing of the first run data from test $MP2500_5$ on sub-sample aliquot SAND1c (Fig. 7). **(a)** Light scattering data (black curve) and corresponding best fits for constant RI values of quartz=1.5, variable ABS values of quartz from 0.01 to 1.00 (colour code in b), and constant RI values of decalcified tap water=1.33. **(b)** Granulometric curves computed from reprocessed data in (a). **(c)** D_{10} percentiles for data in the 5 curves illustrated in (b). **(d)** D_{50} percentiles for data in the 5 curves illustrated in (b). **(e)** D_{90} percentiles for data in the 5 curves illustrated in (b). **(f)** Modal values for data in the 5 curves illustrated in (b). It is worth noting that changing also ABS of quartz produces negligible changes in the reprocessed data.

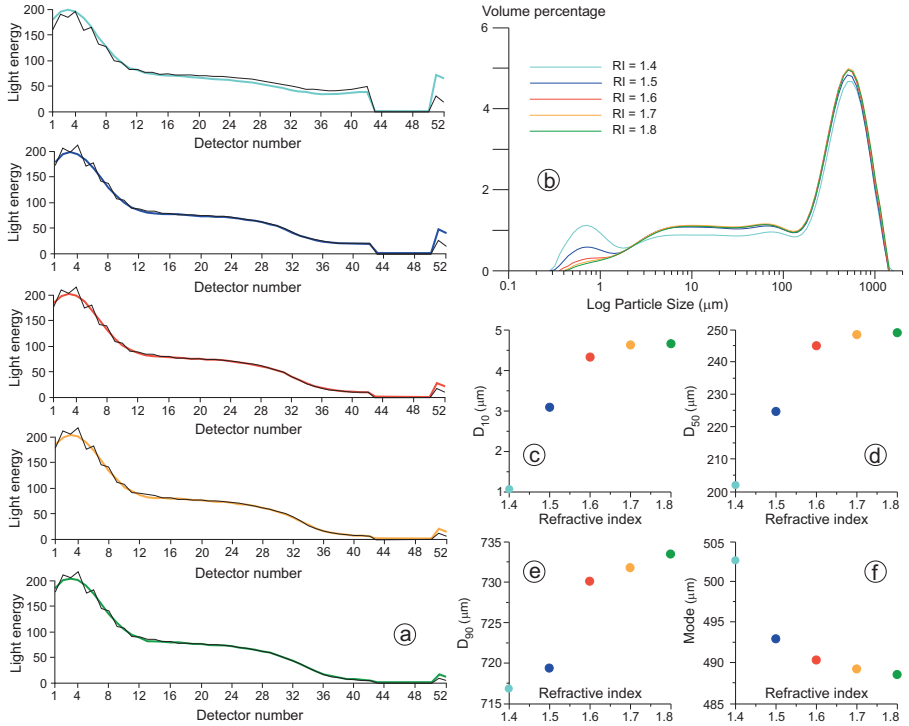

Fig. 21. Reprocessing of the first run data from test MP2000$_5$ on sub-sample aliquot CABRE3d (Fig. 8). **(a)** Light scattering data (black curve) and corresponding best fits for variable RI values of calcium carbonate from 1.4 to 1.8 (colour code in b), constant ABS values of calcium carbonate=0.1, and constant RI values of decalcified tap water=1.33. **(b)** Granulometric curves computed from reprocessed data in (a). **(c)** D_{10} percentiles for data in the 5 curves illustrated in (b). **(d)** D_{50} percentiles for data in the 5 curves illustrated in (b). **(e)** D_{90} percentiles for data in the 5 curves illustrated in (b). **(f)** Modal values for data in the 5 curves illustrated in (b).

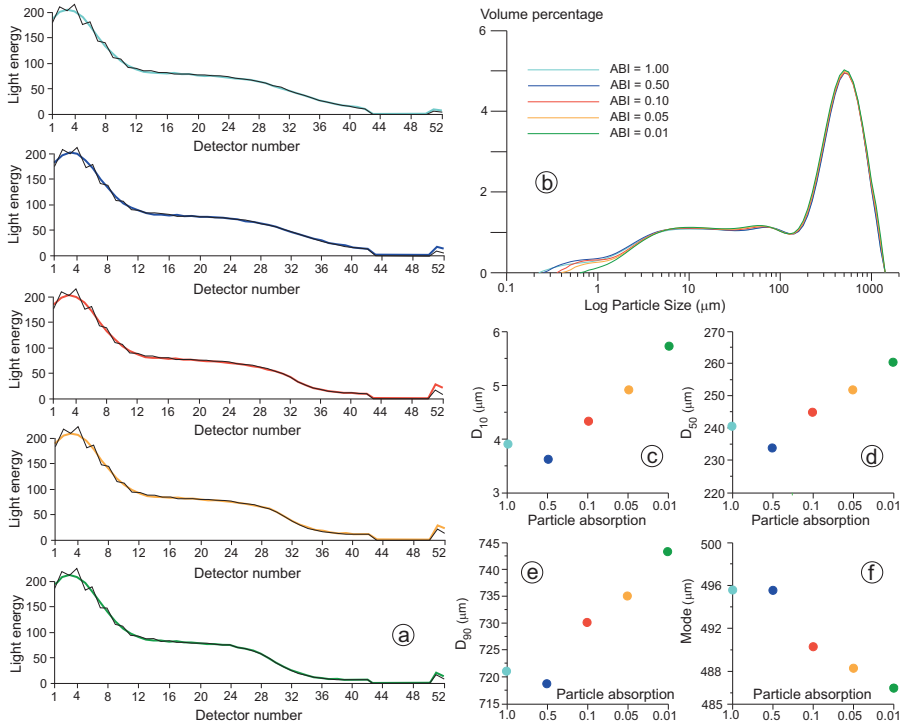

Fig. 22. Reprocessing of the first run data from test $MP2000_5$ on sub-sample aliquot CABRE3d (Fig. 8). **(a)** Light scattering data (black curve) and corresponding best fits for constant RI values of calcium carbonate=1.6, variable ABS values of calcium carbonate from 0.01 to 1.00 (colour code in b), and constant RI values of decalcified tap water=1.33. **(b)** Granulometric curves computed from reprocessed data in (a). **(c)** D_{10} percentiles for data in the 5 curves illustrated in (b). **(d)** D_{50} percentiles for data in the 5 curves illustrated in (b). **(e)** D_{90} percentiles for data in the 5 curves illustrated in (b). **(f)** Modal values for data in the 5 curves illustrated in (b).

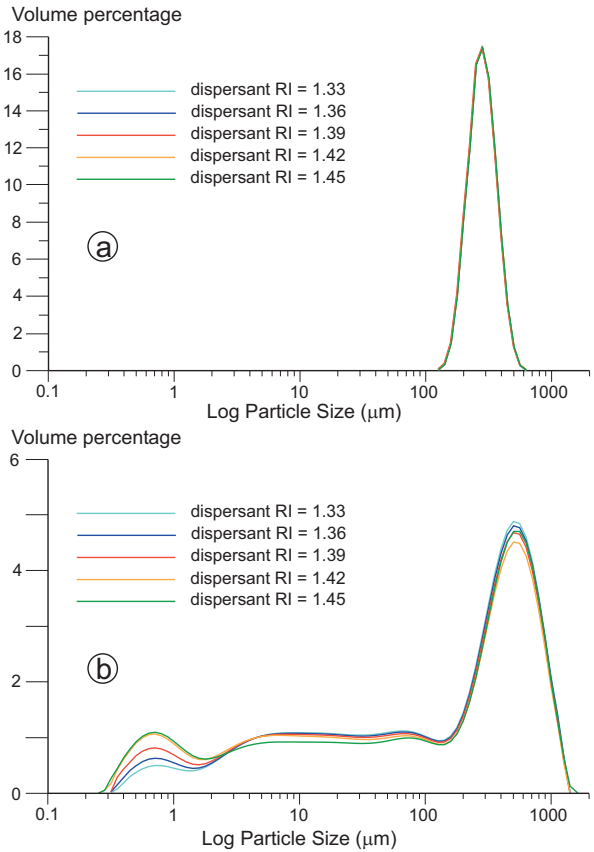

Fig. 23. **(a)** Granulometric curves obtained by reprocessing the first run data from test $MP2500_5$ on sub-sample aliquot SAND1c (Fig. 7) using quartz RI=1.5, quartz ABS=0.1, and variable RI values of decalcified tap water from 1.33 to 1.45. **(b)** Granulometric curves obtained by reprocessing the first run data from test $MP2000_5$ on sub-sample aliquot CABRE3d (Fig. 8) using calcium carbonate RI=1.6, quartz ABS=0.01, and variable RI values of decalcified tap water from 1.33 to 1.45.

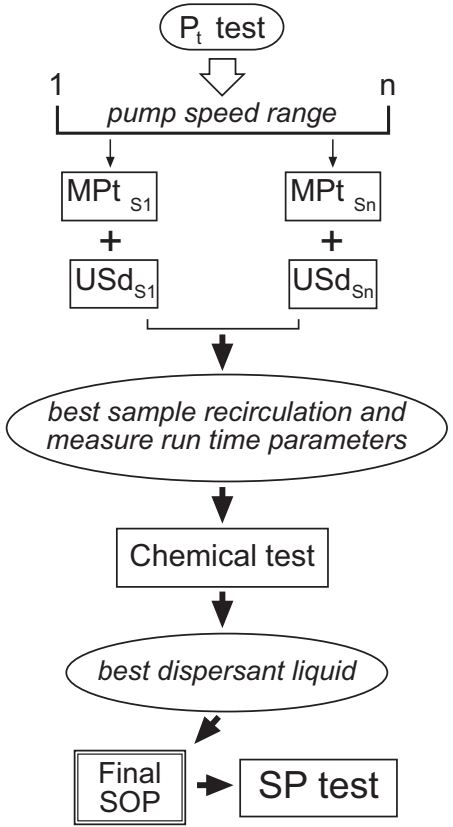

Fig. 24. Flow chart illustrating the main steps that constitute the proposed workflow to select the most appropriate operating procedure for analyzing cataclastic rocks. See text for details.